AJNR

Quantitative high-resolution measurement of cerebrovascular physiology with slip-ring CT.

L M Hamberg, G J Hunter, E F Halpern, B Hoop, G S Gazelle and G L Wolf

AJNR Am J Neuroradiol 1996, 17 (4) 639-650
http://www.ajnr.org/content/17/4/639

Quantitative High-Resolution Measurement of Cerebrovascular Physiology with Slip-Ring CT

Leena M. Hamberg, George J. Hunter, Elkan F. Halpern, Bernard Hoop, G. Scott Gazelle, and Gerald L. Wolf

PURPOSE: To implement and validate spiral slip-ring CT for use in cerebrovascular studies. **METHODS:** Continuous data were acquired from an experimental, first-pass, iodine contrast, bolus study by unidirectional X-ray tube rotation, and images were reconstructed at 100-millisecond intervals. Functional maps of cerebral blood volume (CBV) and cerebral blood flow (CBF) were constructed with voxel-by-voxel gamma variate fitting. Reproducibility studies, different injection volumes and sites, and CO_2 challenge were applied to verify the technique. **RESULTS:** Average absolute cortical gray and white matter and basal ganglia results were reproducible within ±0.8 mL/100 g for CBV and ±20 mL/100 g per minute for CBF. CBV response to changing arterial CO_2 tension was significant only in cortical gray matter and basal ganglia; CBF response was significant in gray and white matter, as well as in the basal ganglia. **CONCLUSION:** Functional CT and constructed functional maps provide an optimal, high-resolution tool with which to visualize cerebrovascular parameters and their changes.

Index terms: Animal studies; Cerebral blood flow; Computed tomography, technique

AJNR Am J Neuroradiol 17:639–650, April 1996

Developments in the quantitative imaging of tissue vascular physiology represent an important contribution to the clinical assessment and care of patients. In many diseases, particularly those of the cerebrovascular system, early alterations in physiological function may signify the advent of morphological changes that are less amenable to treatment. For this reason, the use of quantitative vascular physiological imaging at the outset of assessment for acute or worrisome pathophysiological conditions has been considered with great interest. Quantitative physiological imaging has the capacity to profile cerebrovascular states, establish a clinical diagnosis, and map therapeutic response throughout treatment.

Since medical practice was introduced to computed tomography (CT) in the l970s, considerable effort has been made to increase its temporal resolution. An early objective of this effort was the application of CT to studies of the physiological problems that underlie clinical manifestations. Although many researchers have attempted to portray organ function by using conventional CT (1–3), the technical limitations in speed for this technique were numerous and complex. A recent advance in the design of CT imagers consists of the use of slip-ring technology to collect a continuous stream of data, thereby overcoming the main limitations of previous scanners for the study of vascular dynamics.

Slip-ring imagers are third- or fourth-generation CT scanners that make use of slip-ring technology to transmit power to the X-ray tube, permitting its continuous unidirectional rotation and data acquisition. The need for back rotation is eliminated by this design, and imaging times are remarkably decreased. If the table is moved at a constant speed as the tube rotates, the X-ray beam will describe a spiral path along the

Received July 13, 1995; accepted after revision October 19.

Presented at the 33rd Annual Meeting of the American Society of Neuroradiology, Chicago, Ill, April 21–27, 1995.

From the Department of Radiology, Center for Imaging and Pharmaceutical Research (L.M.H., G.J.H., E.F.H., G.S.G., G.L.W.), and the Pulmonary and Critical Care Unit, Medical Services (B.H.), Massachusetts General Hospital, Boston.

Address reprint requests to Leena M. Hamberg, PhD, Department of Radiology, Center for Imaging and Pharmaceutical Research, Second Floor, Room 2329, Bldg 149, 13th Street, Charleston, MA 02129.

AJNR 17:639–650, Apr 1996 0195-6108/96/1704–0639

body. Owing to the volumetric nature of the acquired information, volumetric reconstruction of spiral CT data is possible. For this reason, slip-ring scanners have generally been used for volumetric or spiral imaging (4, 5). In the present study, however, we modified the application of slip-ring CT technology to facilitate tracking of a bolus of X-ray attenuating contrast agent during its first cerebral circulation in order to generate quantitative maps of cerebrovascular physiology.

Our goals in this work were to exploit and verify the capabilities of slip-ring CT technology to be used in the construction of quantitative, physiological cerebral images. In a rabbit model, we evaluated methods for determining cerebral blood volume (CBV) and cerebral blood flow (CBF), measured the response of these parameters to physiological challenge, and showed that our results are reproducible. To differentiate this technique clearly from dynamic CT applications performed with older, conventional technology, we use the term *functional CT* to refer to physiological, or functional, CT imaging with slip-ring technology.

Materials and Methods

CT Imaging

Continuous data acquisition and image reconstruction. Slip-ring CT technology was used as follows. We continuously rotated the X-ray tube, but kept the table stationary. This allowed data of a high temporal resolution to be obtained from a single section of interest during the initial pass of a contrast agent through cerebral tissue. Each 360° rotation took 1 second, and the total study acquisition time was 50 seconds, corresponding to 50 rotations. From the continuous raw data series thus obtained, it is possible to reconstruct 1-second images at arbitrary time intervals. That is, the reconstruction of each 1-second image can begin as quickly as 1 millisecond after the starting point for the image reconstruction of the previous image. In our study, the reconstruction of sequential images was begun at 100-millisecond intervals. This yielded an effective imaging rate of 10 frames per second. This, in turn, allowed us to measure the changes in contrast agent concentration that occurred in each voxel over sequential 100-millisecond intervals. Another way to view this reconstruction technique is to consider it as a 1-second moving average updated at 100-millisecond intervals.

Brain CT protocol. Imaging was performed on a nutate/rotate Toshiba (Tokyo, Japan) TCT-900S/X-II whole-body CT scanner according to the following imaging protocol. The anesthetized animal was placed supine in the gantry of the scanner, and its position secured with a head holder. Coronal sections in the middle of the brain were prescribed from a lateral scout image. The imaging parameters for all the studies included 120 kV X-ray tube voltage, 150 mA tube current, and high-resolution imaging mode. This resulted in the collection of over 4 million data samples during a 360° tube rotation lasting 1 second. A 1-mm section thickness and a 12-cm field of view, together with a 512 × 512 image matrix, yielded 0.055 mm^2 in-plane resolution. Continuous scanning by unidirectional rotation of the X-ray tube around the object began 5 seconds before the bolus injection of the contrast agent. Scanning was maintained during injection and continued for a total of 50 seconds. Injections were administered with a power injector (Medrad Mark IV, Medrad, Pa).

Animal Model

Animal studies were conducted under the guidelines of the Massachusetts General Hospital Subcommittee on Research Animal Care. Ten healthy New Zealand white rabbits (2.5 to 3.5 kg) were anesthetized by using a mixture of ketamine (40 mg/kg) and xylazine (5 mg/kg) injected intramuscularly. Anesthesia was maintained by hourly injections of pentobarbital (0.25 mg/kg). The left ventricle (via the carotid artery) and/or femoral vein was catheterized for administration of the contrast agent. The femoral artery was catheterized for blood gas determinations. Iohexol (350 mg/mL) iodinated contrast agent (Nycomed, Wayne, Pa) was used for all studies.

Reproducibility studies. To confirm the reproducibility of the technique, we repeated the studies under similar physiological conditions. The same dose and injection site were used, and multiple injections were administered to the same animal. Three animals were used for these studies. Two animals were given intravenous boluses of contrast agent (1.5 mL/kg at 3 mL/s, and 1.7 mL/kg at 5 mL/s). One of these animals received three injections; the other received five. In the third animal, left ventricular injections (1.6 mL/kg at 3 mL/s) were repeated five times. In all cases, a 15-minute time interval was used between sequential first-pass studies. The absolute variation in vascular cerebral parameters was determined from the standard deviation. The relative dispersion (ie, the coefficient of variation) was also determined.

Injection sites and injection volumes. The effects of different injection volumes and injection sites (venous and intraventricular) were studied in four animals. Venous injections were administered into the femoral vein; intraventricular injections into the left ventricle. Three of the four animals were given two intraventricular and two intravenous injections. The exception was given one intravenous and two intraventricular injections. Intraventricular injection rates were 10 mL/s, and contrast agent doses varied from 1.6 to 3.75 mL/kg of total body weight. Femoral venous injection rates were 3, 4, and 5 mL/s and the same dose range was used as that described for arterial injections. The absolute and relative variation in vascular cerebral parameters was determined.

Physiological challenge. The ability of functional CT to measure responses in cerebral perfusion caused by

changes in arterial carbon dioxide tension (P_{CO_2}) was tested in four animals. The CO_2 challenge was used because of its known effects on CBV and CBF (6–8). The test was performed by changing the inhaled gas mixture and by using hyperventilation and/or hypoventilation, facilitated by mechanical ventilation. All contrast agent injections were administered into the left ventricle. Three animals received contrast agent doses of 1.4 mL/kg, and one animal received a dose of 1.9 mL/kg; all injections were administered at a rate of 3 mL/s. Two animals received four injections, one animal received five injections, and one animal received six injections.

Arterial blood samples were drawn immediately before and after every data collection, and the arterial tension of CO_2 and O_2, as well as blood pH (37°C), were measured for each sample by using a blood gas machine (AVL990S, AVL, Graz, Austria). The average CO_2 value from these samples was used to represent the CO_2 tension during data acquisition. The achieved arterial CO_2 values ranged from 24 to 75 mmHg. The relationships between arterial CO_2 and CBV and CBF were determined by using a general linear model analysis for cortical gray matter, white matter, and basal ganglia. This method of analysis takes into account animal-to-animal variations.

The linearity of the measured signal changes as a function of contrast agent concentration for our scanner was established, and signal intensity–time curves were converted into absolute iodine concentration–time curves by using external standards (9).

Data Analysis

Calculation of cerebral blood volume and blood flow. The calculation of CBV and CBF is based on the use of an intravascular contrast agent and the central volume principle. (The Appendix provides a detailed derivation of the central volume principle, based on a stochastic approach.) This makes use of the concept of populations of fluid elements, each characterized by a distribution of times calculated from the instant when an element enters into the flow system under consideration.

In summary, the central volume principle states that blood flow (F) through a system is the ratio of the vascular volume (V) of the system and the mean transit time ($\bar{t}$) of contrast agent through the system

$$1) \qquad F = \frac{V}{\bar{t}}.$$

In our study, we first determined the tissue blood volume on the basis of measured time–concentration curves by normalizing the tissue response function with the arterial input function, as detailed below. The blood flow was then calculated by using the mean cerebral transit time.

Derivation of absolute blood volume. Let us assume a closed system. That is, the total input flow is known; the distribution of distal vessels follows a self-contained branching tree structure; there are no tributaries; and the total output flow is also known. In such a closed system, it follows by conservation of mass that the flows in the arterial input, capillary bed, and venous output are equal. Furthermore, the concentration of contrast agent in blood is also equal throughout the system. Let us assume further that our imaging interval is such that we do not observe the same particle of the contrast agent more than once. Then the following relationship is valid:

$$2) \qquad \int_0^\infty C_A(t)dt = \int_0^\infty C_C(t)dt = \int_0^\infty C_V(t)dt,$$

where C_A, C_C, and C_V are the arterial, capillary, and venous blood concentrations of contrast material, respectively. If C_A is measured from a voxel that is pure blood, then we can define C_C in terms of the tissue voxel concentration (C_T) by introducing a factor, f, which is the fraction of whole blood in a tissue voxel. That is, $C_T = f*C_C$, and Equation 2 becomes

$$3) \qquad \int_0^\infty C_A(t)dt = \frac{1}{f}\int_0^\infty C_T(t)dt.$$

This in turn may be rearranged to

$$4) \qquad f = \frac{\int_0^\infty C_T(t)dt}{\int_0^\infty C_A(t)dt}.$$

This is the fractional blood volume in a voxel, expressed in terms of the area under the time–concentration curve in the tissue divided by the area under the time–concentration curve in the arterial input. This fractional blood volume may be converted into absolute blood volume (milliliters of blood in 100 g of tissue) by using knowledge of the voxel volume. There are three caveats to these statements. First, Equation 4 is valid only for the initial passage of contrast material; recirculation must be eliminated from consideration. Second, an estimation of tissue density must be provided to convert voxel volume to voxel mass. Third, all the tissue enhancement is assumed to be caused by the contrast agent within the blood rather than by contrast material extravasated from the vascular space. This assumption holds only if the blood-brain barrier is intact.

Derivation of absolute blood flow. According to the central volume principle, tissue blood flow (usually referred to as *tissue perfusion*) may be calculated by dividing the tissue blood volume (milliliters of whole blood per 100 g of tissue) by the mean transit time. In this study, we determined the mean cerebral transit time by measuring the difference in mean transit times observed in the common carotid artery and sagittal sinus.

Construction of functional maps. A series of images was obtained during the first circulation of a bolus of contrast agent through cerebral tissue. From these images, the change in contrast agent concentration, measured as the change in Hounsfield units (ΔHU), was obtained and converted to a time–concentration curve. This curve was con-

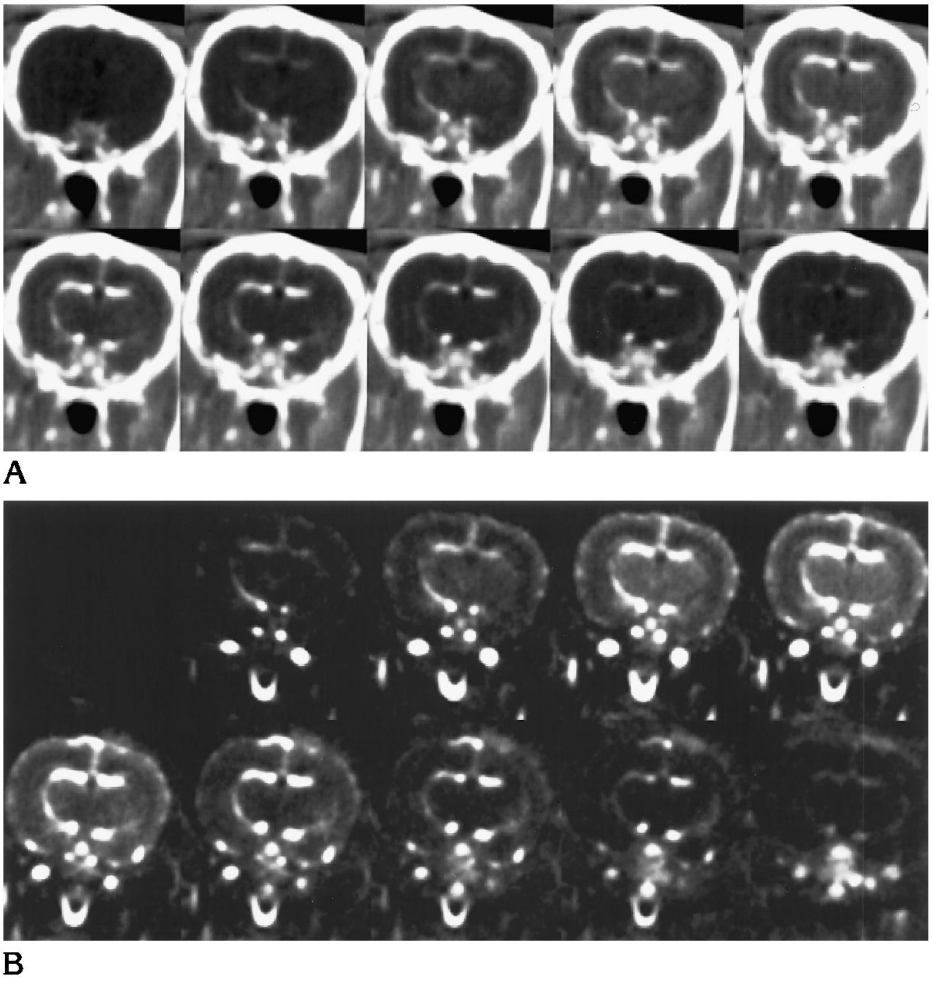

Fig 1. Temporal series of 1-second conventional (HU) images with a 1-second time interval between sequential images.

A, The distinction between gray and white matter caused by differences in blood volume and flow becomes apparent when the contrast agent concentration in the blood is highest.

B, Reference-subtracted (ΔHU) images reflecting the actual iodine concentration in each voxel. This series was reconstructed from the images shown in *A* by baseline reference image subtraction. Note the greater clarity of vascular structures in the ΔHU images.

structed for each voxel. To remove the effect of recirculation, we fit gamma variate functions (9, 10) to these curves, and the area under each fitted curve was calculated with custom software (First Pass, Elite Software Co, Halisham, East Sussex, United Kingdom). In those cases in which the contrast agent remains entirely intravascular, the area under each fitted curve is proportional to the tissue blood volume fraction in the corresponding voxel, as indicated in Equation 4. By presenting the areas as a parametric image, we generated a regional relative CBV map.

In an ideal case, in which injection of the indicator is at the input and its observation is at the output of the system under investigation, the time–concentration curves observed at the output represent frequency distributions of the contrast agent's transit times through the system (11, 12). The first moment of such a transit time frequency distribution gives the mean transit time through the system (13). This measurement is not available to us. In our experiments, we observe the tissue response of a particular voxel rather than its output. If we calculate the first moment of the tissue response curve, we obtain the sum of well-understood time intervals with the zero time point as the start of image acquisition. Thus, we observe the duration of baseline imaging before the contrast agent is injected, followed by the duration of time when the contrast material travels from the injection site to the voxel of interest, and finally the duration of residency of the contrast material within the voxel under study. The first two components cannot usually be separated without additional, independent information. However, the residency time may be obtained from our analysis. This is achieved by independently calculating the arrival time of contrast material in the voxel and subtracting it from the first moment of the voxel (14). This process is performed for each voxel, and the resulting tissue residency time is presented as a color-coded functional map. If we assume that the actual input to each voxel is derived from a common input (an assumption that is valid in the context of a closed system as described above), then differences in voxel residency times reflect relative differences in tissue transit times (tTT). For each voxel, if we divide the CBV by the tTT, we can obtain an index of relative CBF (CBFi). This index of CBF reflects local variations in blood flow within the brain, and may also be presented as a functional image.

The relative CBV map can be converted into an absolute measurement by applying Equation 4, if the contrast

concentration in the arterial input can be identified in the imaged section. The image-based definition of the arterial input function makes the functional CT method noninvasive, apart from the contrast agent injection. We were able to identify the common carotid, internal carotid, and middle cerebral arteries in all animals studied, allowing conversion to absolute units to be performed.

Results

An example of a timed image series is presented in Figure 1A. Each image is reconstructed from raw data obtained during 1-second rotation of the X-ray tube, with a 1-second time interval between sequential images. From these studies, the distinction between gray and white matter becomes apparent as the bolus of contrast agent passes through the brain. Regional differences in signal intensities are caused by variable iodine concentrations that result from different blood volume and blood flow values in gray and white matter voxels. Figure 1B shows the conversion of the temporal image series into a series that reflects actual iodine concentration in the voxels. This is achieved by constructing an average baseline reference image from those images in the series acquired before the arrival of the contrast material and by subtracting this reference image from each subsequent image. The differences in the behavior of the contrast material in differing vascular structures are better appreciated in these reference-subtracted (ΔHU) images than in conventional (HU) images.

Figure 2 shows a representative set of time–concentration curves obtained from gray and white matter, as well as from the middle cerebral artery and sagittal sinus. Here, the time interval between sequential points on the curves is 100 milliseconds. This figure illustrates that the tissue phase of the passage of contrast material through the brain lies between the arterial and venous phases, as expected.

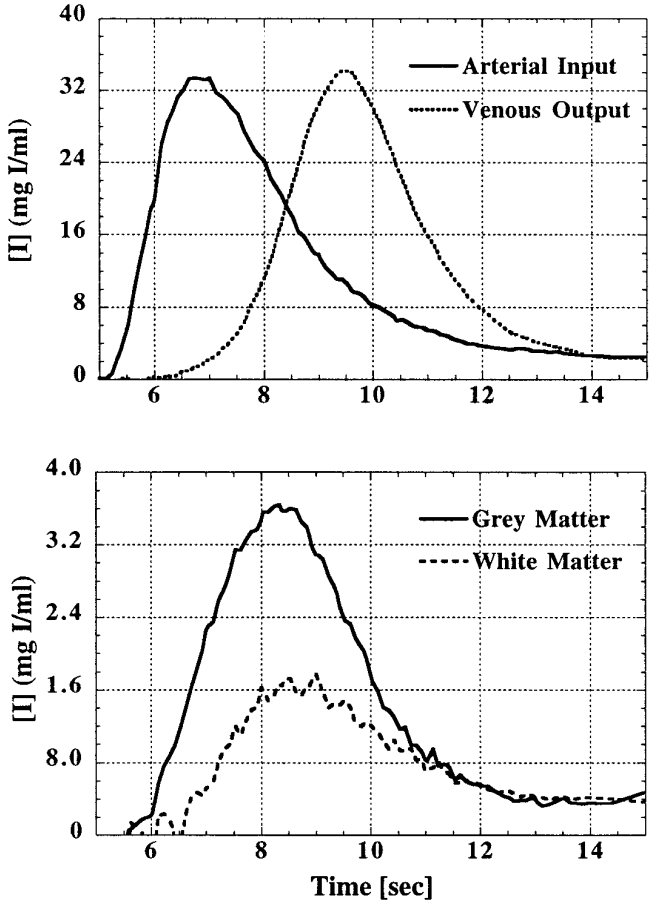

Fig 2. A representative set of time–concentration curves for cortical gray matter, white matter, common carotid artery, and sagittal sinus. The time interval between sequential points is 100 milliseconds. Note that the tissue phase lies between the arterial and venous phases, as expected.

Reproducibility Studies

There were 13 data sets from three animals, as described above. The average cerebral mean transit time was 2.3 seconds ± 0.5, with a 14% coefficient of variation. The calculated mean and standard deviations for absolute blood volume and flow determinations, together with their relative dispersions, are shown in Table 1. The measurements of absolute blood volume were reproducible within 0.4 mL/100 g in each of the tissues studied. The blood flow range (95 to 112 mL/100 g per minute) and average variation (19 mL/100 g per minute) that we observed are comparable to the microsphere studies reported in the literature for this species (8, 15).

Injection Sites and Injection Volumes

In Figure 3 the data for intravenous and intraarterial injections are shown for CBV (Fig 3A) and CBF (Fig 3B) in cortical gray matter, white matter, and basal ganglia. There was no difference in CBV or CBF between the two injection sites in any of the anatomic regions studied. Variability in our data (0.5 mL/100 g in CBV and 17 mL/100 g per minute in CBF) was observed to be similar to values obtained in our reproducibility studies. This indicates that data quantitation is independent of injection site, and that the effects of changing injection volumes can be

TABLE 1: Reproducibility of cerebral blood volume (CBV) and cerebral blood flow (CBF) measurements (n = 13)

	Gray Matter	White Matter	Basal Ganglia
CBV, mean ± SD (mL/100 g)	4.1 ± 0.4	3.3 ± 0.4	3.9 ± 0.4
Coefficient of variation	9%	12%	11%
CBF, Mean ± SD (mL/100 g per minute)	111.7 ± 21.5	95.0 ± 14.7	108.9 ± 21.7
Coefficient of variation	19%	17%	19%

corrected. There were 15 data sets in four animals, as described earlier. The average cerebral mean transit time of the contrast agent was 2.9 seconds ±0.9, with an average coefficient of variation of 12%. The mean and standard deviations calculated for absolute blood volume and flow determinations, together with their relative dispersions, are shown in Table 2.

Physiological Challenge

In Figure 4, the responses observed in cerebral vascular parameters subsequent to changes in systemic arterial CO_2 tension are shown for different regions of the brain. CBV was significantly correlated with P_{CO_2} in cortical gray matter ($P < .0001$) (Fig 4A) and in the basal ganglia ($P < .02$) (Fig 4C). In white matter, there was no significant correlation between CBV and P_{CO_2} ($P < .09$) (Fig 4B). There was also no evidence of animal-to-animal variation in the relationship between CBV and P_{CO_2}. Regression lines for percentage of CBV responses to the changes in systemic arterial CO_2 tension were as follows (slope and intercept estimates are followed by their standard deviation): CBV = 0.08 (±0.01) P_{CO_2} + 3.61 (±0.61) for gray matter; CBV = 0.02 (±0.01) P_{CO_2} + 3.02 (±0.48) for white matter; and CBV = 0.04 (±0.02) P_{CO_2} + 3.64 (±0.80) for the basal ganglia.

The pooled data showed that CBF was significantly correlated with P_{CO_2} in all three anatomic locations: gray matter ($P < .0009$), white matter ($P < .02$), and basal ganglia ($P < .002$) (Fig 4D–F). However, a significant animal-to-animal variation was noted in the slopes of this relationship in gray matter ($P < .01$) and in the basal ganglia ($P < .04$). In gray matter, the slopes of the regression lines for the four animals were 4.7 ± 0.7, 4.1 ± 1.4, 1.8 ± 1.0, and 0.3 ± 1.4 mL/100 g per minute. Similarly, in the basal ganglia, the slopes were 2.8 ± 1.3, 0.4 ± 1.3, 1.3 ± 0.9, and 3.4 ± 0.6 mL/100 g per minute. The regression line for CBF responses in white matter was CBF = 1.2 (±0.5) P_{CO_2} − 15.7 (±21.0). The CBF regression line, calculated from pooled data, for gray matter was 3.1 (±0.8) P_{CO_2} − 10.9 (±36.1); for the basal ganglia it was 2.1 (±0.6) P_{CO_2} + 5.6 (±26.8).

Functional Maps

Figure 5 shows two sets of functional images. The first set (Fig 5A) provides an example of CBV, the CBF index, tissue residency time, and arrival time maps constructed from a bolus tracking, first-pass imaging study. Note the differences in the arrival times between the left and right sides of the brain. In this animal, the arterial catheter was placed in the right common carotid artery, which may have resulted in a partial delay in the delivery of contrast agent to the right hemisphere. The second set (Fig 5B) illustrates the changes observed in absolute blood volumes, following alteration in P_{CO_2} levels, in a single animal. Here, the shift toward higher values in the frequency histograms of blood volume occurs when the P_{CO_2} increases from 24 mmHg to 62 mmHg.

Discussion

We have presented an implementation of spiral, slip-ring CT, which we have called *functional CT*. We have shown that functional CT is a valuable tool with which to obtain dynamic studies of cerebrovascular physiology and that the technique is able to demonstrate the rapid changes in CBF and CBV resulting from the manipulation of arterial carbon dioxide tension. The derived functional maps provide images of quantitative regional parameters and offer a powerful diagnostic tool for the investigation of vascular disorders.

The technique was reproducible, as indicated by the 9% variation in CBV and the average 18% coefficient of variation in measured CBF. These results compare favorably with data obtained by other researchers who used other techniques (8, 15). Further, no significant variation was

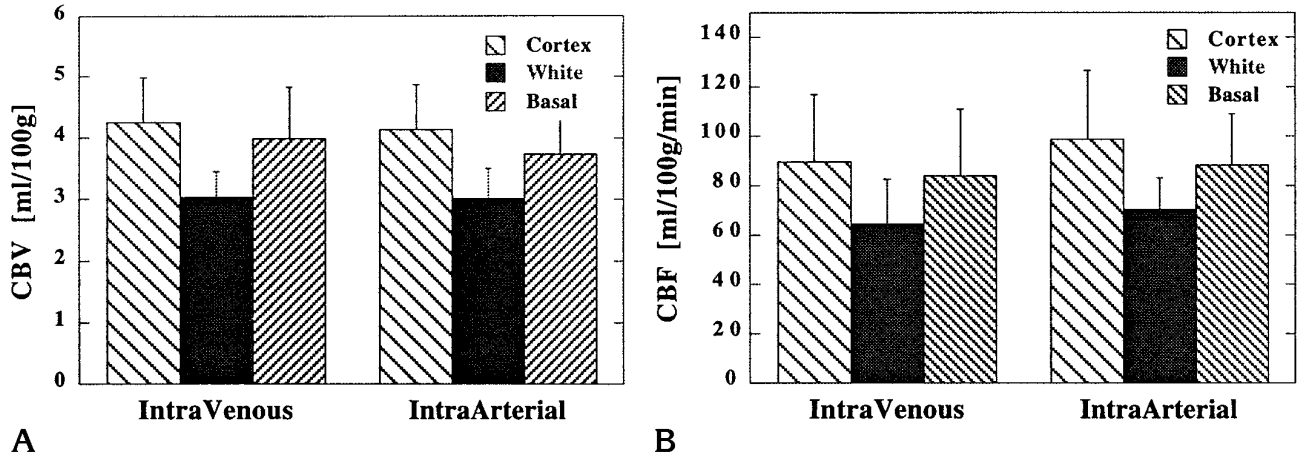

Fig 3. Cerebral blood volume (*CBV*) (*A*) and cerebral blood flow (*CBF*) (*B*) intravenous and intraarterial injection values, obtained under the same physiological conditions. No difference based on injection site was observed in either the CBV or the CBF values for any anatomic region studied (gray matter, white matter, basal ganglia).

TABLE 2: Reproducibility of cerebral blood volume (CBV) and cerebral blood flow (CBF) measurements with intraarterial and intravenous bolus injections (n = 15)

	Gray Matter	White Matter	Basal Ganglia
CBV, mean ± SD (mL/100 g)	4.3 ± 0.6	3.1 ± 0.4	3.9 ± 0.5
Coefficient of variation	14%	13%	13%
CBF, Mean ± SD (mL/100 g per minute)	100.8 ± 23.4	72.7 ± 15.3	91.2 ± 11.3
Coefficient of variation	23%	21%	12%

observed in these numbers for differing injection sites or volumes of injectant.

In our results, a change in CBV of 0.07 mL/100 g, 0.02 mL/100 g, and 0.04 mL/100 g per mmHG changes in arterial P_{CO_2} was observed for gray matter, white matter, and basal ganglia, respectively. Further, our CBF and CBV response curves matched the results from several studies reported in the literature (7, 8, 16). In particular, direct comparison of results from identical regions (gray matter, white matter, and basal ganglia) was possible with MR imaging data reported by Moseley et al, and revealed similar CO_2 reactivity values, reflected in the slopes of the respective CBV and CBF lines, calculated from their raw data (17). In general, the results we report are from more homogeneous regions of interest because the superior spatial resolution of functional CT (0.05 mm^2 in plane) permitted us to exclude confounding large vessels from our analysis and to separate interdigitating areas of gray and white matter with greater accuracy.

The imaging of vascular physiology with functional CT is now feasible through the use of sophisticated CT technology, greatly improved temporal resolution in CT scanners, and state-of-the-art computing capability. The quantitation of temporal functional CT data, however, is based on an application of tracer kinetic theory. In general, tracer kinetic techniques may be applied to any dynamic series of images to obtain quantitative or semiquantitative physiological parameters if five key conditions are satisfied (11). The first of these is that the spatial resolution of the instrument must be sufficiently high to permit local anatomy of interest to be identified separately from undesired surrounding or overlying tissues. Second, the temporal resolution of the detection system must be able to resolve time-variant changes in the physiological process under study. The third condition requires that the relationship between the measured signal and tissue contrast concentration be uniquely defined. Fourth, the indicator that is used must reflect the physiology of interest without perturbing it. Finally, the physiological process under study should be in a steady state throughout the period of measurement.

Functional CT of the brain fully meets all of the tracer kinetic requirements described above, except for the condition that requires an indicator to reflect physiology without perturbing it, which it only partially satisfies. Violation

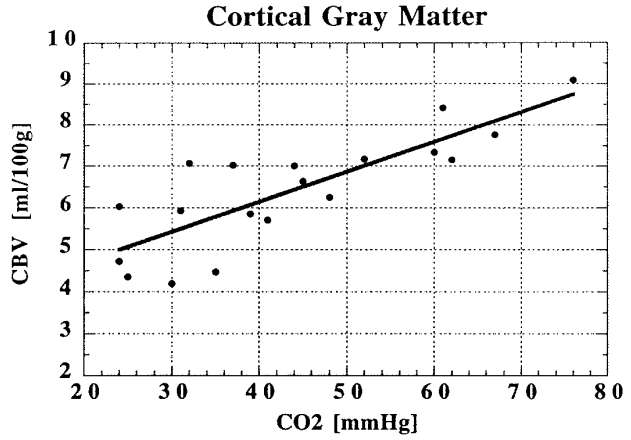

$CBV = 0.08(\pm 0.01)pCO_2 + 3.61(\pm 0.61)$

A

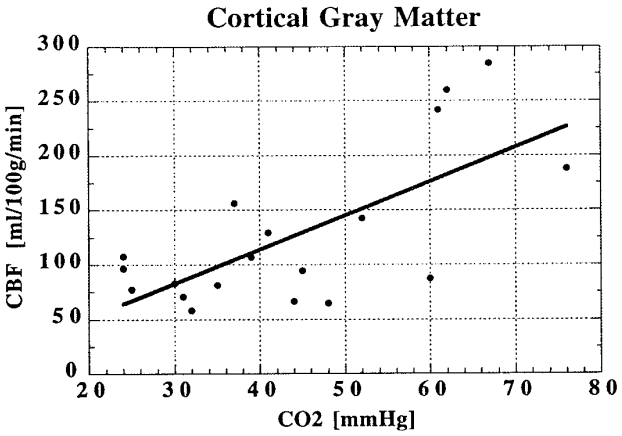

$CBF = 3.1(\pm 0.8)pCO_2 - 10.9(\pm 36.1)$

D

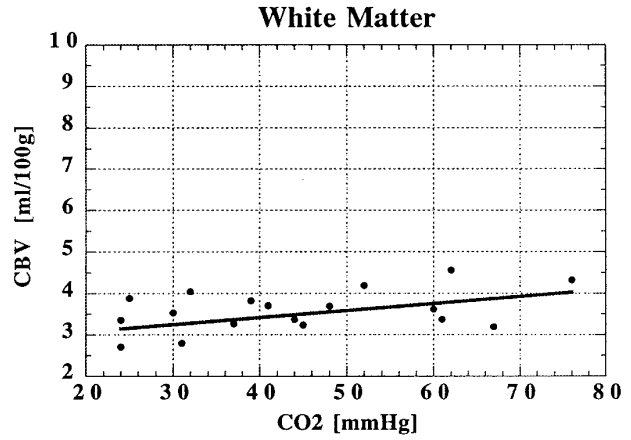

$CBV = 0.02(\pm 0.01)pCO_2 + 3.02(\pm 0.48)$

B

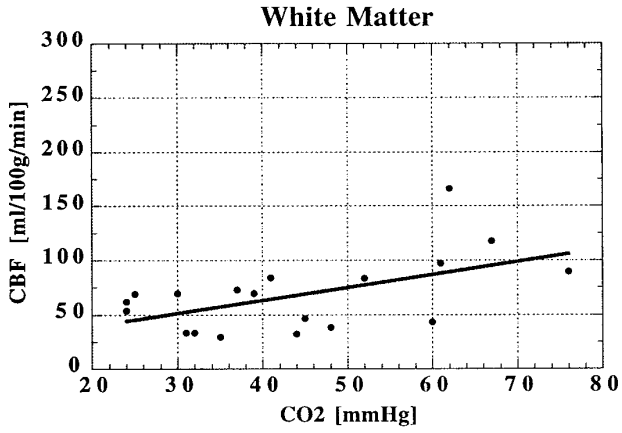

$CBF = 1.2(\pm 0.5)pCO_2 - 15.7(\pm 21.0)$

E

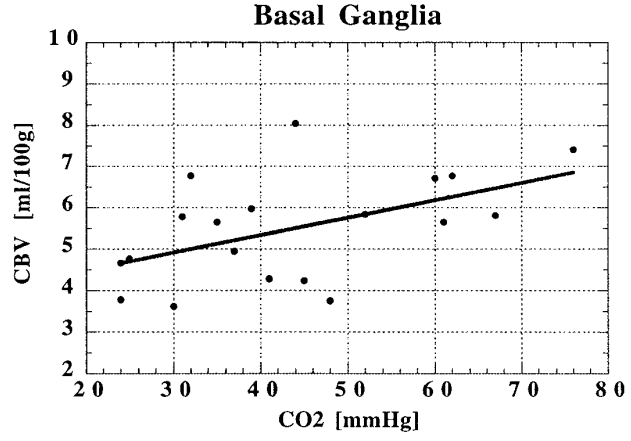

$CBV = 0.04(\pm 0.02)pCO_2 + 3.64(\pm 0.80)$

C

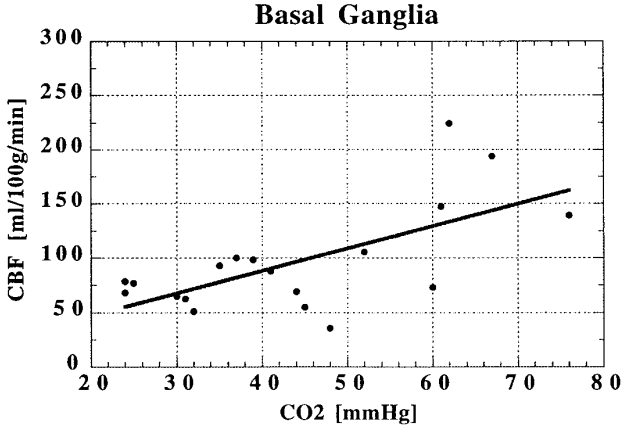

$CBF = 2.1(\pm 0.6)pCO_2 + 5.6(\pm 26.8)$

F

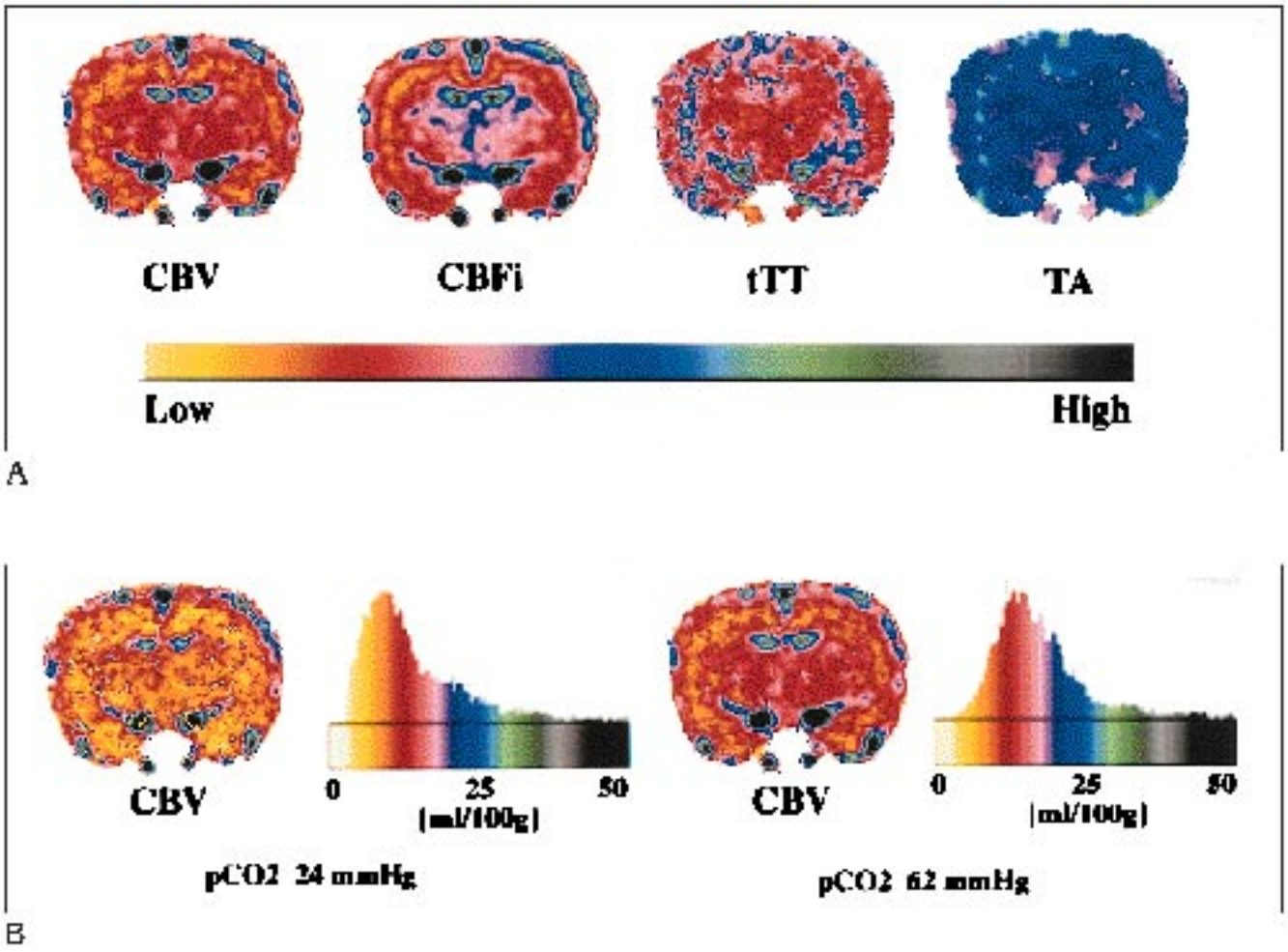

Fig 5. An example of cerebral blood volume (*CBV*), cerebral blood flow index (*CBFi*), tissue residency time (*tTT*), and arrival time (*TA*) maps constructed from a bolus-tracking, first-pass imaging study (*A*). Also illustrated (*B*) are the changes observed in absolute blood volumes after alteration in P_{CO_2} levels in a single animal. Note the shift in the frequency histograms of blood volume toward higher values when the P_{CO_2} increases from 24 mmHg to 62 mmHg.

of this condition may occur, for example, if a large dose of hyperosmolar contrast agent is used, resulting in a transient alteration in the distribution of tissue water due to the high osmolar gradients. This effect can be minimized, however, and in most situations is effectively eliminated, by the use of isoosmolar contrast agents.

Currently, functional CT is limited to the acquisition of a single section, although simultaneous multisection capability is already available in some manufacturers' spiral CT scanners. In addition, multiple sections can be imaged through sequential data collections and contrast agent boluses. The time window for one continuous functional CT data acquisition, as well as the time interval required between sequential studies, is limited in these cases by the X-ray tube heat capacity and its cooling properties. The system used in the present

Fig 4, *opposite*. Gray matter (*A*), white matter (*B*), and basal ganglia (*C*) responses in cerebral blood volume (*CBV*) as a function of changing arterial CO_2. In the areas of gray matter ($P < .0001$) and basal ganglia ($P < .002$), a significant response can be seen. In the white matter, however, no significant correlation between CBV and P_{CO_2} could be measured ($P < .09$). The cerebral blood flow (*CBF*) was significantly correlated with changing arterial CO_2 tension in all three anatomic locations. In cortical gray matter (*D*) and basal ganglia (*F*), a significant animal-to-animal variation in the response was noted. In white matter (*E*), the response was the same for all four animals. The high spatial resolution permitted with functional CT (in this study, 0.05 mm^3) allowed us to avoid larger vessels in the analysis, resulting in data that reflect cerebral vascular physiology occurring at the capillary level.

study had an X-ray tube with a 3.5-MHU heat capacity and a 732 kHU/min cooling rate; this made it possible to perform 50-second continuous data acquisitions with a 150-mA tube current. However, for clinical cerebral studies, a higher current would be needed to achieve an acceptable signal-to-noise ratio. Increases in tube current would affect the available data acquisition time window in an inverse manner: the higher the current, the shorter the time window. New high-heat-capacity X-ray tubes will alleviate this constraint.

Because safe, approved CT agents are available for use as indicators, functional CT may be easily adopted for clinical use. Multiple injections may also allow sequential studies to be performed. In organ systems other than the brain, the extravasation of contrast agent molecules into the extravascular, extracellular space occurs with the use of currently approved contrast agents. Where this occurs, the quantitation of blood volume and flow becomes more complicated, as the model must account for capillary permeability and movement of the contrast agent through the capillary membrane. The availability of intravascular agents would allow the techniques described in this work to be applied to first-pass investigations of organs that exhibit capillary permeability to current, clinically available contrast agents.

Obvious comparisons between susceptibility contrast MR imaging and functional CT can be made easily with respect to presence or absence of ionizing radiation, relative risks of gadolinium-based and iodine contrast agents, section orientation, and scanner availability. Any of these factors may be crucial in determining the appropriate technique for a specific study. However, the superior spatial and temporal resolution provided by functional CT, together with the fully understood physics of CT and the linearity this technique provides between signal changes and tissue contrast concentration, make functional CT the desirable method to use in the quantitative evaluation of intracranial vascular physiology.

At present, functional CT may easily be applied in clinical studies. On the basis of the results of our investigation, we conclude that this new imaging technique is highly suitable for situations in which particular spatial accuracy and/or quantification of vascular parameters is required. Obvious clinical applications for functional CT include investigations of vascular pathophysiology, studies of tumor vascularity, demonstration of acute stroke, and measurement of vascular parameters in small localized areas (18). The technique is especially suitable for experimental models that are used to investigate new drug therapies or temporal responses in vascular pathophysiology. As effective therapies for stroke become available, and the distinction between hemorrhagic and occlusive stroke is thus made more critical, the ability to quantitate lesion volume and monitor perfusion changes will become more important. Functional CT, because it is based on the measurement of blood flow, has the potential to provide the earliest indication of cerebral occlusion and its distribution. The technique may also demonstrate perfusion gradients as well as the presence or absence of stroke penumbra. Finally, functional CT may prove useful in situations in which the manipulation of P_{CO_2} levels is used to improve cerebral perfusion so as to minimize the volume of ischemic tissue, such as after trauma to the head.

In conclusion, we have demonstrated a new method for the in vivo measurement of cerebrovascular physiology by using existing CT technology that is based on spiral, slip-ring CT. We have shown that the results are reproducible and are valid in an animal model. Further studies will help evaluate the utility of functional CT in a clinical setting.

Acknowledgments

We express our appreciation for the contributions on behalf of this work made by Diane Kierstead and Kathy Tabor McEwan, and for the fine efforts of the entire technical staff at the Center for Imaging and Pharmaceutical Research. We also thank JoAnne Fordham for her invaluable help in preparing the manuscript.

Appendix

Derivation of the Central Volume Principle

The central volume principle follows logically from stochastic descriptions of the transfer of injected material through a system. More important, it can be derived explicitly by using the probability density function of the residency time of fluid elements within a system. The use of a stochastic approach does not require knowledge of the detailed structure of a system, and thus no information is needed about the variations of concentration from point to point within a vessel (12, 19). The populations of indicator elements are characterized by the volume-averaged age

distributions, where the age of a particle of contrast agent is defined as the time that has elapsed since it has entered a flow system (12).

Model used. We define our general flow system as a region of space that is bounded by a surface (imaginary or real) through which mass transport occurs by bulk flow. We assume that the flow rate is sufficiently high to consider as negligible the effects of mass transport by diffusion, and thus to omit them from the calculations. Let us consider a branching system that consists of one common input, many intermediate flow paths, and one common output. If there are many inflows, either they all must meet and mix at the input to the system, or the amount of tracer injected into the different inflows must be in proportion to the flow rate at a given inflow. The latter is the concept of equivalent labeling, and we may assume it to hold true for functional CT studies (as it does for microsphere studies). Thus, the assumption of a single common input is not strictly necessary under these circumstances. Detection of the residue function allows the system to be treated as a single-outlet system (11).

Let Vo be the volume fraction of the system through which there is a steady flow rate, Fo. New fluid continually displaces old fluid from the system. Time zero is set to be the time when a contrast element enters the system; age is calculated from this moment. Any fluid element that enters Vo after time zero is called new; old fluid is the fluid that was already present in the system at time zero.

We then make use of probability density functions of age; namely, the internal age distribution function, I(t), and the external age distribution function, E(t). The internal age distribution function, I(t), is the probability density function of ages of fluid elements within the system; and the external age distribution of fluid from a system, E(t), is the probability density function of the ages of fluid elements that have flowed through and just exited the system. Since I(t) and E(t) are defined as probability density functions, by definition they are normalized such that

$$1) \qquad \int_0^\infty I(t)dt = \int_0^\infty E(t)dt = 1.$$

The mean transit time may therefore be calculated as the first moment of E(t), as follows:

$$2) \qquad \int_0^\infty tE(t)dt = \bar{t}.$$

The actual derivation of the central volume principle may be performed by using the relations between internal and external age distribution functions along the lines of Larson (12). At time $t = t'$, the amount of the new fluid in the volume Vo is $Vo\int_0^t I(t')dt'$. The rate at which the new fluid has been accumulating in the system may be obtained by differentiation, giving $VoI(t)$. Simultaneously, when new fluid is pouring into the system, old fluid is leaving at the volumetric rate, which is equal to the new fluid accumulation rate:

$$3) \qquad V_oI(t) = F_o\int_0^\infty E(t')dt'.$$

An equivalent relationship may be obtained by differentiation of Equation 3:

$$4) \qquad \frac{dI(t)}{dt} = -\frac{Fo}{Vo}E(t).$$

In order to express $\bar{t}$ in terms of system parameters Vo and Fo, we multiply Equation 4 by t and integrate it, giving

$$5) \qquad \int_0^\infty t\frac{dI(t)}{dt} = -\frac{Fo}{Vo}\int_0^\infty tE(t)dt.$$

Equation 5 may be written

$$6) \qquad \int_0^\infty t\,\frac{dI(t)}{dt}dt = -\frac{Fo}{Vo}\bar{t}.$$

By integrating, the left-hand side by parts, we obtain

$$7) \qquad \int_0^\infty t\,\frac{dI(t)}{dt}dt = tI(t)\,|_0^\infty - \int_0^\infty I(t)dt = -1.$$

As the value of tI(t) is 0 when t approaches infinity, we may write Equation 6 as

$$8) \qquad \bar{t} = \frac{Fo}{Vo},$$

which is the central volume principle.

References

1. Dobben GD, Valvassori GE, Mafee MF, Berninger WH. Evaluation of brain circulation by rapid rotational computed tomography. *Radiology* 1979;133:105–111
2. Berninger WH, Axel L, Norman D, Napel S, Redington RW. Functional imaging of the brain using computed tomography. *Radiology* 1981;138:711–716
3. Norman D, Axel L, Berninger WH, et al. Dynamic computed tomography of the brain: techniques, data analysis, and applications. *AJNR Am J Neuroradiol* 1981;2;1–11
4. Rigauts H, Marchal G, Baert AL, Hupke R. Initial experience with volume CT scanning. *J Comput Assist Tomogr* 1990;14:675–682
5. Fishman EK, Jeffrey RB. *Spiral CT: Principles, Techniques and Clinical Applications.* New York, NY: Raven Press, 1995:1–227
6. Kety SS, Schmidt CF. The effects of altered arterial tensions of carbon dioxide and oxygen on cerebral blood flow and cerebral oxygen consumption of normal young men. *J Clin Invest* 1948; 27:484–492
7. Grubb RL, Raichle ME, Eichling JO. The effects of changes in $PaCO_2$ on cerebral blood volume, blood flow, and vascular mean transit time. *Stroke* 1974;5:630–639.
8. Lacombe P, Meric P, Seylaz J. Validity of cerebral blood flow measurements obtained with quantitative tracer techniques. *Brain Res Rev* 1980;2:105–169

9. Thompson HK, Stramer CF, Whalen RE, McIntosh HD. Indicator transit time considered as a gamma variate. *Circ Res* 1964;14: 502–515
10. Axel L. Cerebral blood flow determination by rapid-sequence computed tomography. *Radiology* 1980;137:679–686.
11. Lassen NA, Perl W. *Tracer Kinetic Methods in Medical Physiology*. New York, NY: Raven Press, 1979:1–186
12. Larson KB. Physical principles of tracer kinetics, In: Larson KB and Cox JR, eds. *Computer Processing of Dynamic Images from an Anger Scintillation Camera*. New York, NY: The Society of Nuclear Medicine, 1971:70–94
13. Lindgren BW. *Statistical Theory*. New York, NY: Macmillan Publishing Co, 1968:50–160
14. Hamberg LM, MacFarlane R, Tasdemiroglu E, et al. Measurement of cerebrovascular changes in cats after transient ischemia using dynamic magnetic resonance imaging. *Stroke* 1993;24:444–451
15. Lo EH, Sun G-H, Steinberg GK. Effects of NMDA and calcium channel antagonists on regional cerebral blood flow. *Neurosci Lett* 1991;131:17–20
16. Traystman RJ. Microcirculation of the brain, In: Mortillaro NA, ed. *The Physiology and Pharmacology of the Microcirculation*. New York, NY: Academic Press, 1983:237–298
17. Moseley ME, Chew WM, White DL, et al. Hypercarbia-induced changes in cerebral blood volume in the cat: a ^{1}H MRI and intravascular contrast agent study. *Magn Reson Med* 1992;23:21–30
18. Hamberg LM, Kristjansen PEG, Hunter GJ, Wolf GL, Jain RK. Spatial heterogeneity in tumor perfusion measured with functional computed tomography at 0.05 μl resolution. *Cancer Res* 1994;54: 6032–6036
19. Jacquez JA. *Compartmental Analysis in Biology and Medicine*. Ann Arbor: University of Michigan Press, 1985:560